Journal of Molecular Structure 1235 (2021) 130230

Contents lists available at ScienceDirect

Journal of Molecular Structure

journal homepage: www.elsevier.com/locate/molstr

Synthesis, crystal structure, molecular docking studies and biological evaluation of aryl substituted dihydroisoquinoline imines as a potent angiotensin converting enzyme inhibitor

Awatef Selmi[a], Rihab Aydi[a], Omar Kammoun[b], Hajer Bougatef[c], Ali Bougatef[c], Nabil Miled[d], Othman A. Alghamdi[d], Majed Kammoun[a,*]

[a] Laboratory of Medicinal and Environment Chemistry, Higher Institute of Biotechnology, University of SFAX, PB 261, 3000 SFAX, Tunisia
[b] Laboratoire Physicochimie de l'Etat Solide, Département de Chimie, Faculté des Sciences de Sfax, Université de Sfax, BP 1171, 3000 Sfax, Tunisia
[c] Laboratory of Plant Improvement and Valorization of Agroressources, National School of Engineering of Sfax (ENIS), University of Sfax, Sfax 3038, Tunisia
[d] Department of biological sciences, College of Science, University of Jeddah- Asfan Road, Kingdom of Saudi Arabia

ARTICLE INFO

Article history:
Received 21 December 2020
Revised 13 February 2021
Accepted 27 February 2021
Available online 6 March 2021

Keywords:
Imines
X-ray structure
Molecular docking
Anti-hypertensive activity

ABSTRACT

The different functionalities of imine group found in many compounds are of important biological activity. Since, the development of novel imines is biologically encouraged, this study aims to develop a straightforward synthesis pathway of dihydroisoquinoline imines that could reveal antihypertensive effects. Starting from 2-méthyl-1-phényl-2-propanol, four different dihydroisoquinoline imines compounds **(2a-d)** were obtained and their structures were analyzed by mass spectrum, elemental analysis and NMR spectral studies. The crystal structure of **2b** was determined from single crystal X-ray diffraction data.

The newly synthesized compounds were evaluated for angiotensin I-converting enzyme (ACE) inhibition, using an enzymatic in vitro assay. The results were compared to Captopril as a reference drug. Compounds **2a, 2b** and **2d** showed inhibition activity with IC_{50} values of **0.15, 0.13** and **0.40** mg/ml, respectively. The docking of chemical compounds in the ACE active site explained the higher inhibitory capability of compounds **2a** and **2b** on the catalytic activity of the enzyme, indicating a potential anti-hypertensive effect of these compounds.

Introduction

Imines (schiff bases), which were first reported by Hugo Schiff in 1864, are compounds with the structure of azomethine group (-C=N-) [1], and represent an important intermediates in the organic synthetic chemistry and fine chemical industry [2-6].

Also, schiff bases represent an important class of organic compounds, especially in the medicinal and pharmaceutical fields. They have shown a broad range of biological activities including antioxidant [7], anticancer [8-9], antimalarial [10], antimicrobrial [11], antifungal [12], antidiabetic [13], anti-obesity [14], and anti-*Leishmania tropica* [15].

There are several methods used to prepare imines, of which is the classical way involving the condensation of active aldehydes and amines, whereas the synthesis of aldehydes is usually time-consuming and expensive [16].

Other approaches have been reported in the literature such as the dimerization, oxidation or dehydrogenation of primary amines, [17-21] and the coupling of alcohols and amines [22-23].

The imine formation is one of the most important reactions in organic and medicinal chemistry [24]. Examples of using imines as versatile components include the asymmetric synthesis of α-aminonitriles [25], preparation of secondary amines by hydrogenation [26], and cycloaddition reactions [27]. Moreover, imines are intermediates in the synthesis of some compounds such as isoxazoline and pyrazolines [28], quinolones [29], α-alkylidene β-oxoamides [30], 1,5-amino/ketoalcohols [31] and oxaziridines [32-36].

Owing to the interesting imines, our research group has been working on an easy and efficient method for the synthesis of schiff bases. Our proposed method shows distinct features such as invovlving, good efficiency, short reaction times and excellent yields.

The aim of this study was twofold: (1) synthesizing four imines, namely **2a-d** with substituents in position 1, including a phenyl and a Parachloro phenyl groups, (2) focusing on the effect of the

* Corresponding author.
E-mail address: majed.kammoun@isbs.rnu.tn (M. Kammoun).

https://doi.org/10.1016/j.molstruc.2021.130230
0022-2860/

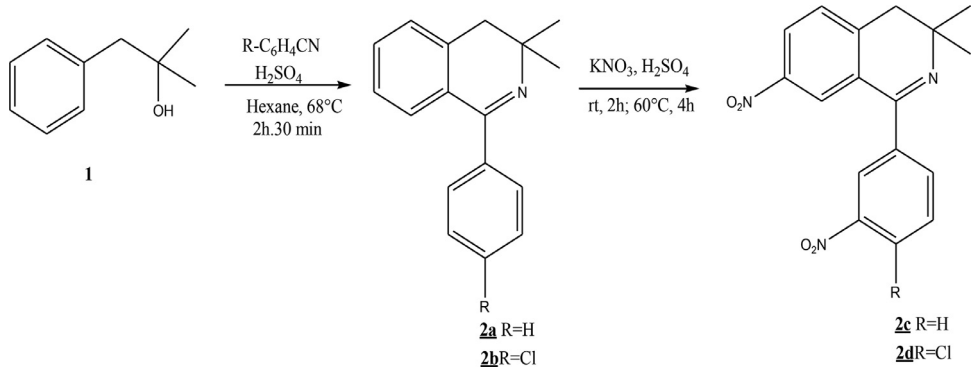

Scheme 1. Synthesis of imines **2a-d**.

introduction of substituents in the aromatic ring on the ACE inhibition activity.

A suitable crystal of imine **2b** was obtained by recrystallization and the molecular structure was confirmed by single X-ray analysis.

The newly synthesized compounds were evaluated for their in vitro ACE inhibition. Molecular docking studies were used to explain their ACE inhibitory power.

2. Results and discussion

2.1. Chemistry

The molecules **2a-d** shown in the current study were synthesized starting from the commercial tertiary alcohol **1**(Scheme1). In the first step, imines **2a-b** were acquired by the acid catalyzed reaction of 2-methyl-1-phenylpropane-2-ol using Ritter–type procedure [37]. The next step included the nitration of these imines **2a-b** under soft conditions [38,39] and selectively directed to their derivatives **2c-d**.

Nuclear magnetic resonance (NMR) spectral analysis is an important analytical technique used to determine the structures of organic compounds.^{1}H and ^{13}C spectral data of all compounds have been presented in SI. The NMR spectroscopy of all synthesized compounds was registered using $CDCl_3$ as a solvent.

The compounds described herein possess an electrondonor and attracter groups which allowed evaluation of substituent effects on ^{1}H and ^{13}C chemical shifts.

In the ^{1}H NMR spectra of imines (**2a-d**), the peak of gem-dimethyl corresponding to the 6 protons was seen as a singlet and the two equivalent neighboring protons of $-CH_2$ group appeared as a singlet.

In the aromatic region, the proton chemical shifts evidenced the electron-donating character of the chlorogroup, herein, chemical shifts were appeared to a lower frequency compared to the derivative with a phenyl group. In fact the aromatic protons are positioned between 7.23–7.61 ppm for **2a** and between 7.16–7.51 ppm for **2a.**

The chemical shifts of protons of the aromatic ring are increased due to the presence of electron attracter group NO_2in the phenyl ring. Indeed the aromatic protons were appeared signals between 7.47–8.48 ppm for **2c** and 7.49–8.32 for **2d** compared with **2a** and **2b**.

In the ^{13}C NMR spectra of these compounds (**2a-d**), the chemical shifts were appeared between 121.5 – 164.5 ppm corresponding to the aromatic ring. And, the aliphatic carbon atoms were shown in the range of 27.3–55.5 ppm. The two carbons of gem-dimethyl were distinguished as one peak.

Furthermore, mass spectrum showed a $[M + H]+$ peak at *m/z* 270,10,349 corresponding to its molecular formula, $C_{17}H_{16}NCl$ (Fig. 1).

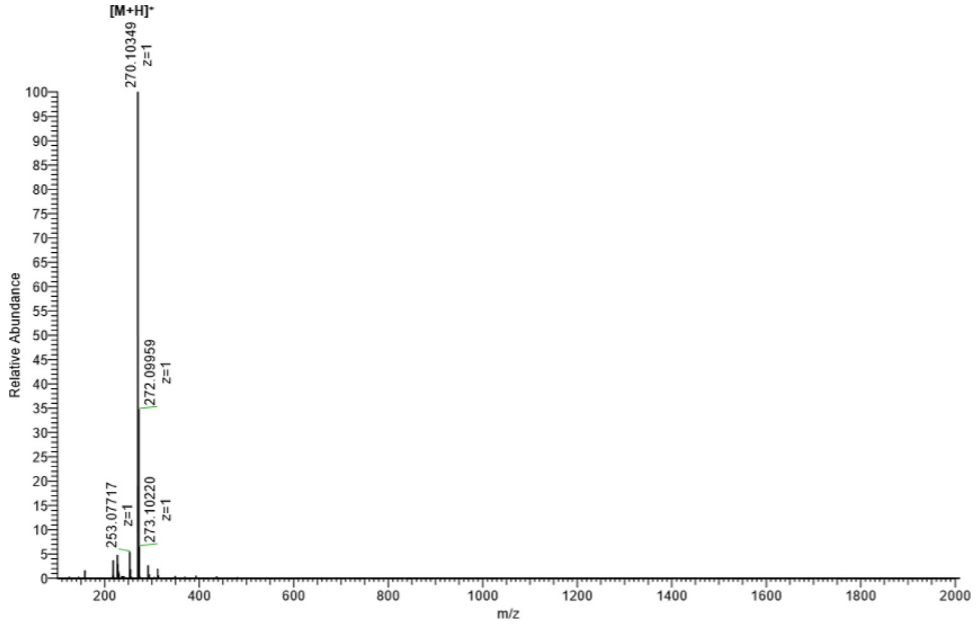

Fig. 1. FT-MS Spectrum of compound 2b.

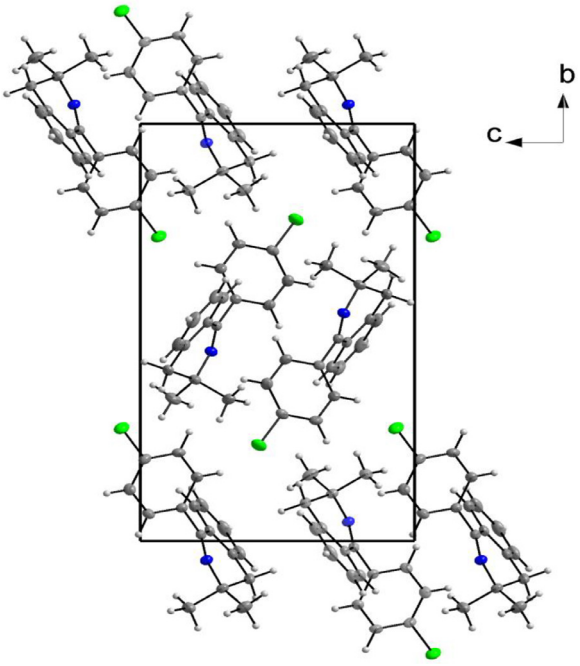

Fig. 2. Crystal packing of $C_{17}H_{16}NCl$ along the crystallographic a axis, showing its supramolecular structure (For clarity, intermolecular hydrogen bonds are omitted).

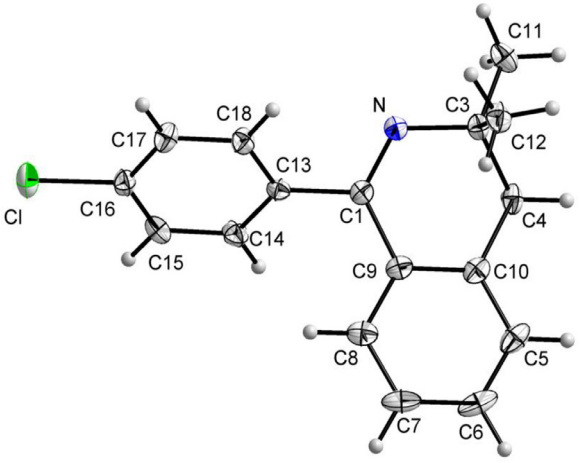

Fig. 3. Molecular structure of the compound 1-(4-chlorophényl) −3, 3-diméthyl −3,4-dihydroisoquinoléine **2b** with atom numbering.

2.2. Crystal structure of 2b

Crystals **2b** were obtained by recrystallization from 1,4-dichlorobutane. The molecular structure of **2b** is shown in Fig. 3. The compound with formula $C_{17}H_{16}NCl$ crystallize in the monoclinic symmetry, with the centrosymmetric space group $P2_1/c$. The crystal structure is built from only the organic imine molecules interconnected between themselves *via* weak hydrogen bonding. Such connectivity defines the supramolecular network of the structure (Fig. 2). Crystallographic data, selected bond lengths and bond angles are listed in Tables 1-2, respectively.

In the molecular structure of **2b**, the tetrahydroisoquinoline unit is substituted by a chloro phenyl ring attached to C1, and two methyl groups attached to C3; the one is pseudo-equatorial and the second is pseudo-axial (Fig. 3).

Table 1
Crystallographic data and structure refinement parameters for **2b**.

Empirical formula	C_{17} H_{16} Cl N
Formula weight	269.76
Temperature	150 K
Wavelength	0.71073 Å
Crystal system, space group	Monoclinic, P 1 2_1/c 1
Unit cell dimensions	a = 8.2804(3) Å, α = 90 °
	b = 17.5586(7) Å, β = 98.6290(10) °
	c = 9.8062(4) Å, γ = 90 °
Volume Z,	1409.61(10) Å^3
Calculated density	4, 1.271 (g.cm^{-3})
Absorption coefficient	0.256 mm^{-1}
F(000)	568
size	0.500 × 0.320 × 0.130 mm
Crystal color	colourless
Theta range for data collection	3.130 to 27.511 °
h_min, h_max	−10, 8
k_min, k_max	−22, 22
l_min, l_max	−12, 12
Reflections collected / unique	17,085 / 3216 [R(int)[a] = 0.0295]
Reflections [$I>2\sigma$]	2811
Completeness to theta_max	0.993
Absorption correction type	multi-scan
Max. and min. transmission	0.967, 0.849
Refinement method	Full-matrix least-squares on F^2
Data / restraints / parameters	3216 / 0 / 174
bGoodness-of-fit	1.028
Final R indices [$I>2\sigma$]	R1[c] = 0.0329, wR2[d] = 0.0828
R indices (all data)	R1[c] = 0.0399, wR2[d] = 0.0881
Largest diff. peak and hole	0.298 and −0.295 e-.Å^{-3}

Table 2
Selected bond distances (Å) and angles (°) for **2b**.

Cl – C16	1.7438(12)	C3 – C11	1.5256(17)
C16 – C17	1.3850(17)	C3 - C12	1.5328(17)
C16 – C15	1.3871(18)	C3 – C4	1.5331(16)
C15 – C14	1.3881(17)	C4 - C10	1.5003(17)
C14 – C13	1.3965(16)	C10 – C5	1.3908(17)
C13 – C18	1.3923(16)	C10 – C9	1.4057(16)
C13 – C1	1.4967(15)	C5 – C6	1.387(2)
C18 – C17	1.3903(17)	C6 – C7	1.385(2)
C1 - N	1.2825(15)	C7 – C8	1.3925(17)
C1 – C9	1.4874(16)	C8 – C9	1.3950(17)
N - C3	1.4830(14)		
C17 – C16 – C15	121.62(11)	C11 – C3 – C12	110.41(11)
C17 – C16 - Cl	119.63(9)	N – C3 – C4	111.86(9)
C15 – C16 - Cl	118.74(9)	C11 – C3 – C4	109.26(10)
C14 – C15 – C16	119.03(11)	C12 – C3 – C4	111.78(10)
C15 – C14 – C13	120.57(11)	C10 – C4 – C3	112.16(9)
C18 – C13 – C14	119.07(11)	C5 - C10 – C9	119.40(12)
C18 – C13 – C1	119.19(10)	C5 – C10 – C4	123.34(11)
C14 – C13 – C1	121.74(10)	C9 - C10 – C4	117.24(10)
C17 – C18 – C13	121.01(11)	C6 – C5 - C10	120.62(13)
C16 – C17 – C18	118.64(11)	C7 – C6 – C5	120.18(12)
N – C1 – C9	124.54(11)	C6 – C7 – C8	119.90(12)
N – C1 – C13	116.52(10)	C7 – C8 – C9	120.34(12)
C9 – C1 – C13	118.80(10)	C8 – C9 - C10	119.54(11)
C1 - N – C3	119.15(10)	C8 – C9 – C1	122.96(11)
N – C3 - C11	106.97(10)	C10 – C9 – C1	117.42(10)
N – C3 – C12	106.42(9)		

The dihedral angle between the plane containing the chloro phenyl attached to C1 and the plane formed by the atoms of the phenyl ring coordinated at C1 and C4 is equal to 63.26° (Fig. 4).

2.3. Hirshfeld surface analysis

To more investigate intermolecular interaction in crystal packing we carry out Hirshfeld surface analysis. The Hirshfeld analysis results are shown in Fig. 5. It is evident that in all potential molecular contacts, hydrogen–hydrogen contacts predominate, contributing 54.1% of the overall intermolecular interactions. The second most significant intermolecular interaction is H···C and H···Cl, re-

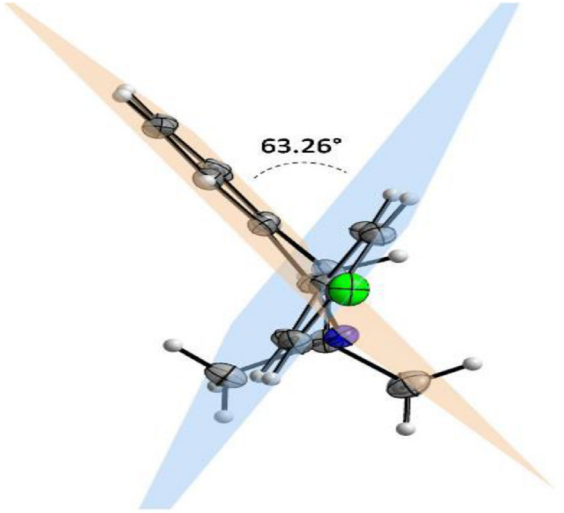

Fig. 4. Projection on planes axes.

sulting in 25% and 16.2% of the sum of intermolecular interactions, respectively. In addition, H···N, C···Cl and C···C interactions also contribute a little to the total intermolecular interactions. In general, the crystal structure is stabilized by a variety of interactions.

2.4. Biological activity

Inactivation of angiotensin converting enzyme (ACE)

Hypertension is one of the largest risk factors associated with mortality worldwide, further accounting for more than half of all cases of stroke and coronary diseases [40]. ACE is an effective therapeutic target for the treatment of hypertension, and commercial ACE inhibitors are common [41].

The inhibition of angiotensin-converting enzyme (ACE) is an important therapeutic approach employed in the treatment of high blood pressure. This enzyme is a widely distributed zinc-dependent metallopeptidase that converts angiotensin I to angiotensin II (vasoconstrictor octapeptide). ACE also promotes the degradation of the vasodilator bradykinin [42].

Several effective oral ACE inhibitors have been developed, namely, captopril, enalapril, and lisinopril and all are currently used as clinical antihypertensive drugs [43]. The in vitro ACE inhibitory activity of newly synthesed compounds were measured using a colorimetric method. Most of the antihypertensive molecules have been characterized by the rabbit lung ACE inhibitor assay, based on the hydrolysis of the synthetic peptide hippurylhistidylleucine (HHL). HHL is hydrolyzed by ACE to hippuric acid (HA) and histidyl-leucine (HL). The extent HA released is directly proportional to the ACE activity.

Table 3
ACE inhibitory activities (IC_{50}) of test compounds and standard drug.

Compounds	**2a**	**2b**	**2d**	**STD.**
IC_{50} (mg/ml)	0.15	0.13	0.40	0.07

Imines derivatives synthesized by our procedure inhibited ACE activity, in a concentration-dependent manner (Fig. 6). Results ACE inhibitory activities (IC_{50}) of imines (**2a-d**) are presented in Table 3.

Furthermore, the inhibitory concentration at 50% (IC_{50}) ACE activity for compounds **2a, 2b, 2c** and **2d** was calculated from dose-response curves (Fig. 6) obtained by plotting the percentage inhibition vs. the concentration.

The evaluation of IC_{50} data for **2a-d** values ranged from 0.13 to 0.4 mg /ml, revealed **2b** as the best lead compound with the lowest IC_{50} (0.13 mg/ml), which was substituted with a chloro group in position 14. This activity was conserved when the imine was substituted with a phenyl group as in **2a** (IC_{50} 0.15 mg/ml). These results also correlate with the IC_{50} values of the reference drug Captopril (0.07 mg/ml), which was expected because Captopril is a drug especially developed for treatment of hypertension.

The presence of a nitro group in 7 and 13 in **2d** caused a reduction of ACE inhibition activity (IC_{50} 0.40 mg/ml). While the absence of inhibition activity from **2c.**

The compound **2b** seems therefore to be a stronger inhibitor of ACE, followed by compound **2a**. Increasing the polarity of the ligand by adding two NO_2 group in ortho positions on the phenyl rings (**2d** compound) diminished ACE inhibitory capacity. Docking experiments were conducted in order to understand this discrepancy.

Docking of inhibitors in the active site of ACE

All ligands were found to bind within the catalytic pocket of the ACE with free binding energies ranging from −9 to −7.9 Kcal/mol. All compounds were located close to the catalytic site (Fig. 7). Compounds **2a** and **2b** were superimposed with an RMSD value of 0.5 Å due to their structural similarity. Compounds **2c** and **2d** are more bulky and their deviations from **2a** orientation were 2.2 and 3.5 Å, respectively. This displacement is explained by the presence of bulky and highly polar NO_2 groups for compounds **2c** and **2d** Introducing polar and bulky NO_2 groups at these positions yielded new polar interactions. Even though compounds **2c** and **2d** are structurally similar, their orientations deviated by 4.5 Å. This is to be explained by the introduction of chloro substituent in **2d** Com-

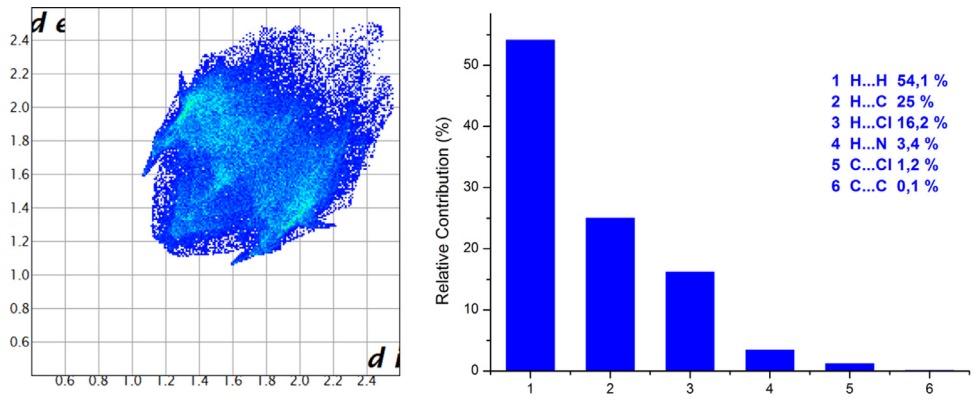

Fig. 5. Hirshfeld surface analysis of $C_{17}H_{16}NCl$.

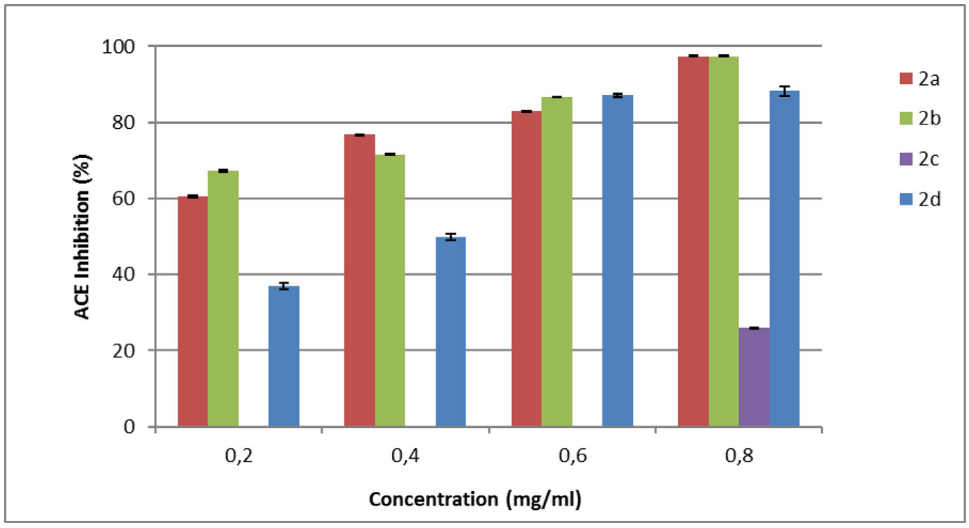

Fig. 6. Dose-dependent angiotensin I-converting enzyme (ACE) inhibition activity of test compounds.

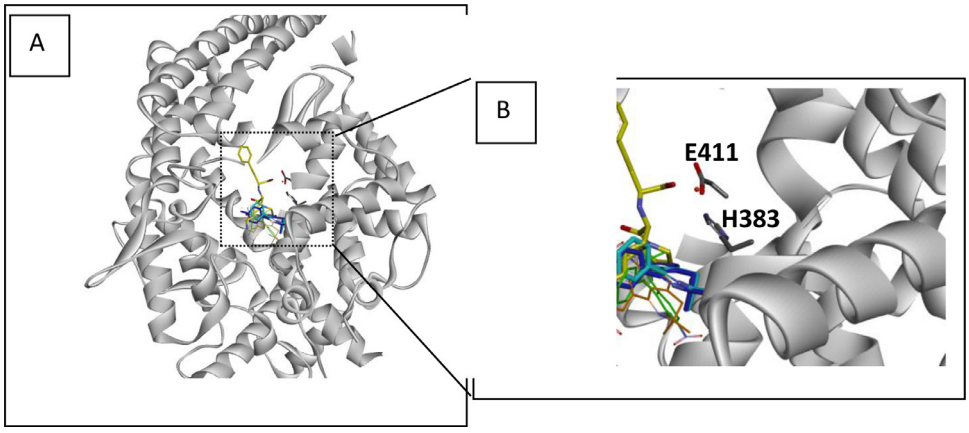

Fig. 7. Complex between the ACE and the best poses corresponding to compounds **2a, 2b, 2c** and **2d,** generated by docking. A, Overall structure of the complex. All compounds and residues were shown as sticks. Catalytic residues playing key role in enzymatic activity were depicted as sticks (H383 and E411). Catalytic Zinc atom bound to H383 and E411 is shown as a red sphere. The lisinopril inhibitor in the active site of ACE (PDB code 1O86) is displayed as yellow wide sticks. **2a** and **2b** are represented as wide sticks whereas **2c** and **2d** as thin sticks. B, Zoom view from A showing the ligands in the active site of ACE. (For interpretation of the references to colour in this figure legend, the reader is referred to the web version of this article.)

pounds were located at distances of 3.5, 3.5, 6.7 and 4.1 Å from catalytic H383 whereas this distance was 3.5 for the lisinopril inhibitor. The catalytic H383 and E411 are interacting with the catalytic zinc ion (Fig. 7). This proximity of imine compounds to H383 might explain their inhibitory effect through preventing the substrate from acceding to the catalytic residues.

Compound **2a** was mainly establishing hydrophobic contacts with residues H353, A354, V379, V380 and catalytic H383 (Fig. 8A and A'). Compound **2b** is superimposed to **2a** and is making similar interactions (Fig. 8B and B'). Compound **2c** is also establishing hydrophobic contacts with V379 and V380 but is not interaction with catalytic H383. Its two NO_2 polar groups are hydrogen bonded to NH groups of residues Q281 and A354 (Fig. 8C and C'). Regarding compound **2d**, it is in hydrophobic contacts with residues P407, H410, F512 and H353. Its NO_2 groups are hydrogen bonded to D358 and Y523. One of its NO_2 groups is interacting with the catalytic zinc (Fig. 8D and D'). Orientations of compounds **2a** and **2b** were similar (RMSD of 0.5 Å). Introduction of polar NO_2 groups for compounds **2c** and **2d** caused them to have different orientations (RMSDs of 2.2 and 3.5 Å, respectively) thus creating new polar interactions. Even though they are structurally similar, introduction of an additional chlore group in compound **2d** changed its orientation as compared to **2c** (RMSD of 4.4 Å). This displacement created new interactions of the chloro substituent with residues H353 and F512 (Fig. 8D and D'). Interestingly, the chloro substituent in both compounds **2a** and **2d** is stabilized by H353. When analyzing interactions of the native inhibitor lisinopril in the active site of ACE, many interactions described for the compounds **2a**-**2d** are reproduced, mainly interactions with catalytic zinc and H353. Lisinopril is making hydrophobic contacts with residues V518 and favorable charge interactions with Y523 and catalytic E411. It is hydrogen bonded to H353, catalytic E411,Y520 and Y523. Its central COO group is interaction with catalytic zinc in a similar way to NO_2 group in compound **2d** Compounds **2a, 2b** and **2d** were located at the same distance range from catalytic histidine as the inhibitor lisinopril (3.5–4.1 Å). The ability of **2a, 2b** and **2d** inhibitors to block the access to the catalytic histidine and zinc ion is in line with their strong inhibitory effect towards the ACE. Compound **2c** located further from catalytic histidine (at a distance of 6.7 Å) displayed a lower in-

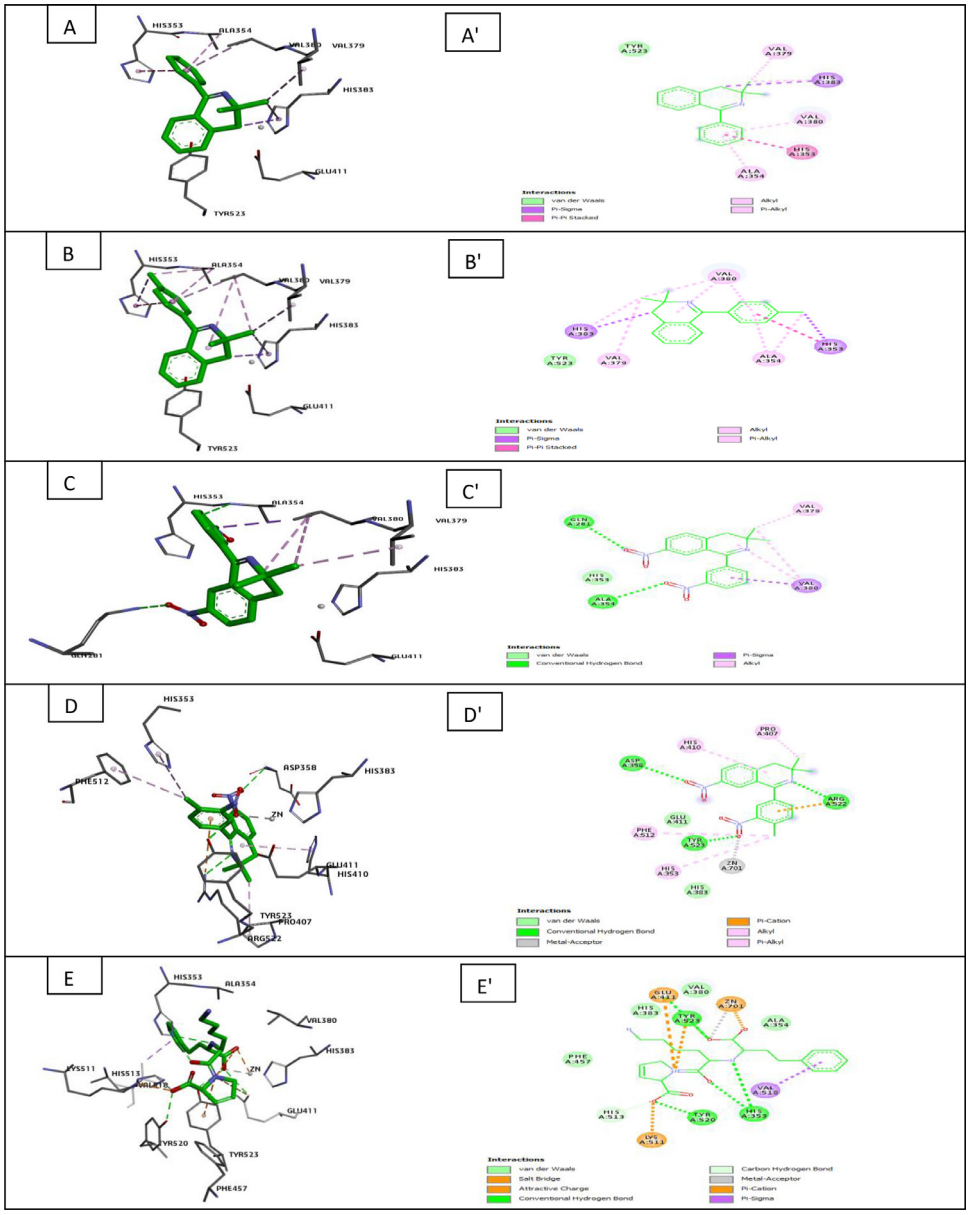

Fig. 8. Interactions of compounds with residues from ACE. Panels A, B, C and D correspond to interacting residues with **2a, 2b, 2c** and **2d**, respectively. Panel E corresponds to lisinopril inhibitor. A', B', C', D', and E' are 2D projections from A, B, C, D and E, respectively. Compounds are shown as wide sticks whereas interacting residues are in thin sticks. Catalytic residues H383 and E411 are depicted as red sticks. Catalytic zinc is shown as red sphere.

hibitory capacity. It is also able to prevent the access of the substrate to the catalytic cavity since it is located in the substrate binding pocket. It can therefore compete with the substrate during binding. These compounds' predicted orientations might be used to design new ACE inhibitors with higher affinity through chemical modifications.

3. Experimental section

3.1. Chemistry

Solvents were purified by standard procedures. Melting points (mp) were determined under a microscope with a Leitz Wet-zlair device and uncorrected. NMR spectra were recorded on an AC 400 Bruker spectrometer at 400 MHz for ^{1}H and 100 MHz for ^{13}C, chemical shifts (δ) were given in ppm and coupling constants (J) were given in hertz (Hz) and abbreviations for multiplicity are respectively called (s = singlet, d = doublet, dd = doublet of doublets, t = triplet, dt = doublet triplet, m = multiplet).

All the reactions were monitored by TLC using commercial silica gel plates and visualization was accomplished by UV light

3.1.1. General synthetic procedure of imines 2 (a-b)

To a cooled (0°) solution, 2 mL of sulfuric acid H_2SO_4 (95%) was added dropwise and under magnetic stirring, to 1.25 eq of (benzonitrile, p-chlorobenzonitrile) in 5 mL of hexane. Then, 500 mg (3.33 mmol) of tertiary alcohol 1 (commercial product) in 5 mL of hexane was added to the solution. After return to room temperature, the resulting mixture was stirred at 68 °C for 2.5 h. The solution was cooled at the room temperature, poured on ice-cold water under magnetic stirring and alkalized with ammonia.

The organic layer was extracted with dichloromethane, washed with a saturated aqueous NaCl solution, dried over sodium sulfate, and filtered. Then, the solvent was removed in vacuo and the obtained crude was purified by chromatography (silica gel, eluent dichloromethane/methanol 98:2). The purity of the products was checked by TLC.

Preparation of imine 2a: 3,3-Dimethyl-1-phenyl-3,4-dihydroisoquinoline. The general procedure was followed using 429 mg (4.162 mmol) of benzonitrile to yield **2a** as a white solid (83%). mp: 69–71 °C. ^{1}H NMR (400 MHz, $CDCl_3$) δ ppm: 1.34 (s, 6H, $2CH_3$), 2.86 (s, 2H, CH_2), 7.23–7.61 (m, 9H, H-Ar). ^{13}C NMR (100 MHz, $CDCl_3$) δ ppm: 27.64, 38.84, 54.49, 126.43, 127.92, 128.00, 128.14, 128.22, 128.78, 128.95, 130.65, 137.54, 139.30, 164.53. HRMS (ESI) [M + *H*]+ calc. For $C_{17}H_{18}N$ 236.1433; found 236.1424.

Preparation of imine 2b:1-(4-Chlorophenyl)−3,3-dimethyl-3,4-dihydroisoquinoline. The general procedure was followed using 572 mg (4.16 mmol) of 4-chlorobenzonitrile to yield **2b** as a white solid (72%): mp 112–115 °C. ^{1}H NMR (400 MHz, $CDCl_3$) δ ppm: 1.27 (s, 6H, $2CH_3$), 2.80 (2H, CH_2), 7.16 (m, 1H-Ar), 7.21 (m, 2H-Ar), 7.39 (m, 3H-Ar), 7.51 (m, 2H-Ar). ^{13}C NMR (100 MHz, $CDCl_3$) δ ppm: 27.56 ($2CH_3$), 38.84 (CH_2), 54.69 (C-$2CH_3$), 126.58, 127.67, 128.40, 130.26, 130.95, 135.10, 137.61, 137.68, 163.61. HRMS (ESI) [*M* + *H*]+ calc. For $C_{17}H_{17}ClN$ 270.1044; found 270.1034.

3.1.2. General synthetic procedure of imines 2 (c-d):

The cold imine **2(c-d)** 600 mg was added dropwise to 6 mL of sulfuric acid (95%). A solution of potassium nitrate (2,3 eq) in 2 mL sulfuric acid was added dropwise whith mainting the temperature at 0 °C. The reaction medium was stirred at room temperature for 2 h, then at 60 °C for 4 h. After return to room temperature, the reaction medium was poured on ice-cold water, and alkalized with ammonia. The organic phase was extracted with dichloromethane, washed with a saturated aqueous solution of chloride sodium, dried over sodium sulfate, filtered and evaporated. The residue was purified by chromatography (silicgel, eluent dichloromethane/ methanol 98:2). The purity of the products was checked by TLC.

Preparation of imine 2c: 3, 3-Dimethyl-7-nitro-1-(3-nitrophenyl)−3, 4-dihydro isoquinoline. The general procedure was followed using 600 mg (2,52 mmol) of **2a** to yield **2c** as a yellow solid (65%). Mp: 172–174 °C. ^{1}H NMR (400 MHz, $CDCl_3$) δ ppm: 1.31 (s, 6H, $2CH_3$), 2.94 (2H, CH_2), 7.47 (d, ^{3}J = 8.1 Hz, 1H-Ar), 7.67 (t, ^{3}J = 8.1 Hz, ^{3}J = 7.5 Hz, 1H-Ar), 7.90 (ddd, ^{3}J = 7.5 Hz, ^{4}J = 1.8 Hz, ^{4}J = 1.2 Hz, 1H-Ar), 7.99 (d, ^{4}J = 2.1 Hz, 1H-Ar), 8.30 (dd, ^{3}J = 8.1 Hz, ^{4}J = 2.1 Hz, 1H-Ar), 8.38 (ddd, ^{3}J = 8.1 Hz, ^{4}J = 2.1 Hz, ^{4}J = 1.2 Hz, 1H-Ar). ^{13}C NMR (100 MHz, $CDCl_3$) δ ppm: 27.38 ($2CH_3$), 38.68 (CH_2), 55.45 (C-$2CH_3$), 121.73, 123.79, 124.59, 126.03, 127.71, 129.75, 134.39, 145.07, 146.94, 148.49, 160.75. HRMS (ESI) [*M* + *H*]$^{+}$ calc. For C17H16N3O4 326.1135; found 326.1121.

Preparation of imine 2d:1-(4–chloro-3-nitrophenyl)−3, 3-dimethyl-7-nitro-3, 4 dihydroisoquinoline. The general procedure was followed using 600 mg (2,22 mmol) of **2b** to yield **2d** as a white solid (93%). Mp: 194–196 °C. ^{1}H NMR (400 MHz, $CDCl_3$) δ ppm: 1.31 (s, 6H, $2CH_3$), 2.94 (2H, CH_2), 7.49 (d, ^{3}J = 8.3 Hz, 1H-Ar), 7.69 (d, ^{3}J = 8.3 Hz, 1H-Ar), 7.74 (dd, ^{3}J = 8.3 Hz, ^{4}J = 2.2 Hz, 1H-Ar), 8.04 (d, ^{4}J = 2.2 Hz, 1H-Ar), 8.19 (d, ^{4}J = 2.2 Hz, 1H-Ar), 8.32 (dd, ^{3}J = 8.3 Hz, ^{4}J = 2.2 Hz, 1H-Ar). ^{13}C NMR (100 MHz, $CDCl_3$) δ ppm: 27.30 ($2CH_3$), 38.69 (CH_2), 55.59 (C-$2CH_3$), 121.54, 125.96, 126.15, 127.36, 128.50, 129.88, 132.11, 132.83, 137.78, 145.11, 147.01, 148.19, 159.77. HRMS (ESI) [*M* + *H*]$^{+}$ calc. For $C_{17}H_{15}ClN_3O_4$ 360.0745; found 360.0734.

3.2. X-ray crystallography

Suitable crystals were mounted on D8 VENTURE Bruker AXS diffractometer. The structure was solved by direct methods using the *SIR97* program [44], and then refined with full-matrix least-square methods based on F^2 (*SHELXL-97*) [45]. All non-hydrogen atoms were refined with anisotropic atomic displacement parameters. H atoms were finally included in their calculated positions. A final refinement on F^2 with 3216 unique intensities and 174 parameters converged at $\omega R(F^2) = 0.0828$ ($R(F) = 0.0329$) for 2811 observed reflections with $I > 2\sigma(I)$.

3.3.Hirshfeld. surface analysis

Hirshfeld surface analysis [46,47] is performed with CrystalExplorer (Version 3.1) [48] to further understand the relative contributions of intermolecular interactions by various molecular contacts in the organic imine.

3.4. Biology

3.4.1. Determination of the angiotensin I-converting enzyme (ACE) inhibition activity

The ACE inhibitory activity was assayed as reported by Nakamura et al. [49]. A volume of 80 µL containing different concentrations (0.2, 0.4, 0.6 or 0.8 mg mL^{-1}) of test compounds was added to 200 µL of 5 mM hippuryl-L-histidyl-lleucine (HHL) and preincubated for 3 min at 37 °C The test compounds and HHL were prepared in 100 mM borate buffer (pH 8.3), containing 300 mM NaCl. The reactions were then initiated by adding 20 µL of 0.1 U mL-1 ACE from rabbit lung prepared in the same buffer. After incubation for 30 min at 37 °C, the enzyme reactions were stopped by the addition of 250 µL of 0.05 M HCl. The liberated hippuric acid (HA) was extracted with ethyl acetate (1.7 mL) and then evaporated at 90 °C for 10 min. The residue was dissolved in 1 ml of distilled water and the absorbance of the extract at 228 nm was determined using a UV–visible spectrophotometer (UV mini 1240, UV/VIS spectrophotometer, SHIMDZU, China).

The average value from three determinations at each concentration was used to calculate the ACE inhibition rate as follows:

$$ACE\ inhibition\ \% = \left(\frac{B-A}{B-C}\right)x100$$

where *A* is the absorbance of HA generated in the presence of ACE inhibitor, *B* is the absorbance of HA generated without ACE inhibitors (100 mM borate buffer pH 8.3 was used instead of compounds **2(a-d)**) and C is the absorbance of HA generated without ACE (corresponding to HHL autolysis in the course of enzymatic assay). The IC_{50} value, defined as the concentration of compounds **2(a-d)** required to inhibit 50% of ACE activity, was calculated for each sample using non-linear regression from a plot of percentage ACE inhibition versus sample concentrations.

3.4.2. Molecular docking of the chemical compounds in the ACE binding site

Docking material. Docking preparation and energy (kcal/mol) calculations of compounds and Angiotensin-I converting enzyme (ACE) were performed by MGL tool and AutoDock Vina software with its scoring function [50-51]. MGL tool is used to generate PDBQT files which are input files to run docking by Vina. In a comparative assessment of scoring functions (CASF) carried out in 2018, popular and free software docking programs AutoDock and Vina were generally in the first half and first quarter, respectively, among all methods tested in CASF-2013. Vina was the best of all methods in terms of docking power [52]. AutoDoc Vina uses a hybrid scoring function that is inspired by X-score [53], which accounts for van der waals forces, hydrogen bonding, deformation

penalty, and hydrophobic effect. In addition, it combines both the conformational preferences of the receptor–ligand complex and experimental affinity measurements to compute its binding energy [51]. Autodock vina allows a manual choice of the atom types for grid maps, calculating grid map files with AutoGrid. Choosing the "search parameters" and clustering the results after docking is no longer necessary, as Vina calculates its own grid maps quickly and automatically and also clusters and ranks the results [51]. Autogrid pre-calculation of the docking compounds was performed by Autodock Vina. The energy grid was performed based on Lamarckian genetic algorithm [53]. Discovery studio 3.5 (BIOVIA, Dassault Systèmes, [Discovery studio], [3.5], San Diego: Dassault Systèmes, [2020]) visualization software was used to perform the virtual analysis of docking sites and to generate figures.

Preparation of receptor and ligands. The three-dimensional structure of human ACE in complex with lisinopril (1O8A.pdb) was derived from the RCSB PDB Protein Data Bank (http://www.rcsb.org/pdb/home/home.do). Water molecules and the inhibitor lisinopril were removed from the receptor file using Discovery Studio3.5 software. The structure was then protonated (non polar hydrogens are merged), charges are added and structure saved in PDBQT file format using MGL tool and Autodock 4.2 software.

Imine compound structures were generated using ChemBio3D Ultra 12.0 software (CambridgeSoft Co., USA), their energy was minimized with the MM2 tools implemented to the software and they are saved in pdb file formats. Gasteiger charges are added, non polar hydrogens are merged and rotatable bonds detected then files are converted to PDBQT format using MGL tool and Autodock 4.2 software.

Docking analysis. Most of docking parameters in Autodock vina are set as default. The number of generated poses was kept 9 and the exhaustiveness of the search was set to 10. A first docking run of **2a, 2b, 2c** and **2d** compounds on the whole enzyme showed their binding into the catalytic cavity. A second docking run was carried out in a box delimiting the catalytic cavity. The docking run was carried out in a box centered on the macromolecule with a radius of 1.00, center coordinates x: 42.852, y: 34.801 and z: 44.944 and box size of x :30 ; y : 40 and z : 30.

The macromolecule was set as rigid while ligand molecules were kept flexible throughout the docking studies. Rotation was possible for all the ligand's rotatable bonds (One torsion for compounds **2a** and **2b** and 3 torsions for compounds **2c** and **2d**). The best ranked docking poses of each chemical compound in the active site of ACE was obtained according to the scores and binding-energy value. The root mean square deviations (RMSDs) between the ligands' orientations were calculated using ligRMSD software [54].

Docking validation. To check the internal variability of docking results due to random seeds of initial positions, three sets of docking were ran for each compound. Maximal RMSD values found were 0.1 Å for **2a, 2b** and **2d** and 0.19 Å for **2c**, calculated using LigRMSD software.

Native ligand Lisinopril present in the protein structure (pdb code 1O86.pdb) was used for re-docking experiments and the generated conformation was checked. RMSD values calculated using ligRMSD software between the original structure and the generated ligand best pose conformation was lower than 2 Å (1.2 Å).

4. Conclusion

In summary, we have described a highly efficient methodology for the synthesis of four imines **2a-d**, which we screened for their ACE inhibition activity. Among them imines **2a** and **2b** exhibited the most potent ACE inhibitors, hence, the introduction of a chloro substituent in the aromatic ring and NO_2 groups have been found to affect the biological properties of Schiff base compounds. The predicted positions of imines were close to the catalytic histidine and zinc ion. This might highlight their efficiency as anti-ACE inhibitors.

The new confirmed crystal structure of compound **2b** can be considered interesting for further modification as antihypertensive agents. Structure base chemical modification can lead to the design of effective anti-hypertensive compounds.

Authors contributions

Author 1: Awatef SELMI
- Planned, Performed the chemistry experiments.
- analyzed spectra and designed molecules.
- Writing, editing and reviewing the manuscript.

Author 2: Rihab AYDI
-Aided in the chemistry experiments.
-Helped in writing the manuscript.

Author 3: Hajer BOUGATEF
- Processed and performed the biological part.
- Made and interpretation of the biological data.
- Helped in writing the biological part.

Author 4: Omar Kammoun
-Verified and helped the X-ray crystallography

Author 5: Ali BOUGATEF
- Verified and helped in supervising the biological part.

Author 6: Nabil MILED
- Realized the molecular docking.
- Revision of the final manuscript.

Author 7: Othman A. Alghamdi
- Revision of the final manuscript.

Author 8: Corresponding author, Majed KAMMOUN
- Conceived the idea, encouraged to investigate, supervised the findings of this work.
- Critical review and revision of the final manuscript.

Supplementary material

Supplementary information file containing data tables of the crystal structure of compound **2b**, spectral (^{1} H and ^{13} C) NMR of compounds **(2a-d)** are available and Crystallographic data for the structure **2b** reported in this paper have been deposited with the Cambridge Crystallographic Data centre, CCDC (2050888).

Declaration of Competing Interest

None

Acknowledgements

This research was supported by the Ministry of Higher Education, Scientific Research and Technology in Tunisia. The authors wish to express their sincere gratitude to Dr Paul Mosset and Dr Thierry Roisnel from ISCR-Rennes for their help to realize the X-ray structure.

Supplementary materials

Supplementary material associated with this article can be found, in the online version, at doi:10.1016/j.molstruc.2021.130230.

References

[1] R.W. Laye, The chemistry of imines, Chem. Rev. 5 (1963) 489–510.
[2] B. Chen, L. Wang, S. Gao, Recent Advances in aerobic oxidation of alcohols and amines to imines, Acs Catal. 5 (2015) 5851–5876.
[3] B. Dutta, S. March, L. Achola, S. Sahoo, J. He, A. Shirazi Amin, Y. Wu, S. Poges, S. Pamir Alpay, S.L. Suib, Mesoporous cobalt/manganese oxide: a highly selective bifunctional catalyst for amine-imine transformations, Green Chem. 20 (2018) 3180–3185.
[4] X. Han, X. Chen, Y. Zou, S. Zhang, Electronic state regulation of supported Pt catalysts dictates selectivity of imines/secondary amines from the cascade transformation of nitroarenes and aldehydes, Appl.Catal.B:Environ. 268 (2020) 118451.
[5] M. Zhang, S. Wu, L. Bian, Q. Cao, W. Fang, One-pot synthesis of Pd-promoted Ce-Ni mixed oxides as efficient catalysts for imine production from the direct N-alkylation of amine with alcohol, Catal. Sci. Technol. 9 (2019) 286–301.
[6] S.V. Samuelsen, C. Santilli, M.S.G. Ahlquist, R. Madsen, Development and mechanistic investigation of the manganese(III) salen-catalyzed dehydrogenation of alcohols, Chem. Sci. 10 (2019) 1150–1157.
[7] S.B. Zangade, A. Shinde, A. Shinde, S. Chavan, S. Chavan, Y. Vibhute, Y. Vibhute, Solvent-free. Environmentally Benign Syntheses of Some Imines and Antioxidant Activity, Orbital - Electron. J. Chem. 7 (2015) 208–214.
[8] A. Doğan, S. Demirci, N.B. Türkmen, A.B. Çağlayan, S. Aydın, D. Telci, E. Kılıç, K. Şahin, C. Orhan, M. Tuzcu, A.I.D. Ekici, F. Şahin, Schiff Base-Poloxamer P85 Combination Prevents Prostate Cancer Progression in C57/Bl6 Mice, Prostate 76 (2016) 1454–1463.
[9] M. Ariyaeifar, H. Amiri Rudbari, M. Sahihi, Z. Kazemi, A.A. Kajani, H. Zali-Boeini, N. Kordestani, G. Bruno, S. Gharaghani, Chiral halogenated Schiff base compounds: green synthesis, anticancer activity and DNA-binding study, J. Mol. Struct. 1161 (2018) 497–511.
[10] A. Walcourt, M. Loyevsky, D.B. Lovejoy, V.R. Gordeuk, D.R. Richardson, Novel aroylhydrazone and thiosemicarbazone iron chelators with anti-malarial activity against chloroquine-resistant and -sensitive parasites, Int. J. Biochem. Cell Biol. 36 (2004) 401–407.
[11] C. Nastasă, D. Vodnar, I. Ionuţ, A. Stana, D. Benedec, R. Tamaian, O. Oniga, B. Tiperciuc, Antibacterial Evaluation and Virtual Screening of New Thiazolyl–Triazole Schiff Bases as Potential DNA-Gyrase Inhibitors, Int. J. Mol. Sci. 19 (2018) 222.
[12] B. Iftikhar, K. Javed, M.S.U. Khan, Z. Akhter, B. Mirza, V. Mckee, Synthesis, characterization and biological assay of Salicylaldehyde Schiff base Cu(II) complexes and their precursors, J. Mol. Struct. 1155 (2018) 337–348.
[13] J. Liu, C. Chen, F. Wu, J. Tang, Study on the synthesis and biological activities of αsubstituted arylacetates derivatives, Bioorg. Med. Chem. Lett. 26 (2016) 1715–1719.
[14] J.W. Zheng, L. Ma, Assessment of silver(I) complexes of salicylaldehyde derivatives-histidine Schiff base as novel α-glucosidase inhibitors, Chinese Chem. Lett. 27 (2016) 283–286.
[15] M. Ikram, S. Rehman, Q. Jamal, A. Shah, Activity on Leishmania tropica of Metal Complexes with NNOO Tetradentate Schiff Base Ligand: kinetic and Thermodynamic Studies from TG-DTA Analysis, J. Chem. Soc. Pakistan. 37 (2015) 869–878 Anti leishmania.
[16] H. Huang, J. Huang, Y.M. Liu, H.Y. He, Y. Cao, K.N. Fan, Graphite oxide as an efficient and durable metal-free catalyst for aerobic oxidative coupling of amines to imines, Green Chem. 14 (2012) 930–934.
[17] J.W. Kim, K. Yamaguchi, N. Mizuno, Heterogeneously catalyzed efficient oxygenation of primary amines to amides by a supported ruthenium hydroxide catalyst, Angew. Chem. Int. Ed. 47 (2008) 9249–9251.
[18] B. Zhu, R.J. Angelici, Non-nanogold catalyzed aerobic oxidation of secondary amines to imines, Chem. Commun. 21 (2007) 2157–2159.
[19] B. Chen, L. Wang, W. Dai, S. Shang, Y. Lv, S. Gao, Metal-free and solvent-free oxidative coupling of amines to imines with mesoporous carbon from macrocyclic compounds, ACS Catal. 5 (2015) 2788–2794.
[20] X. Qiu, C. Len, R. Luque, Y. Li, Solvent less oxidative coupling of amines to imines by using transition-metal-free metal–organic frameworks, Chem Sus Chem. 7 (2014) 1684–1688.
[21] C. Sarkar, S. Pendem, A. Shrotri, D.Q. Dao, P. Pham Thi Mai, T. Nguyen Ngoc, D.R. Chandaka, T.V. Rao, Q.T. Trinh, M.P. Sherburne, J. Mondal, Interface engineering of graphene-supported Cu nanoparticles encapsulated by mesoporous silica for size-dependent catalytic oxidative coupling of aromatic amines, ACS Appl. Mater. Interfaces 11 (2019) 11722–11735.
[22] X. Huang, L. Liu, H. Gao, W. Dong, M. Yang, G. Wang, Hierarchically nanostructured $MnCo_2O_4$ as active catalysts for the synthesis of N-benzylideneaniline from benzyl alcohol and aniline, Green Chem. 19 (2017) 769–777.
[23] B. Chen, J. Li, W. Dai, L. Wang, S. Gao, Direct imine formation by oxidative coupling of alcohols and amines using supported manganese oxides under an air atmosphere, Green Chem. 16 (2014) 3328–3334.
[24] A. Saber, M. Driowya, S. Alaoui, H. Marzag, L. Demange, E. Álvarez, R. Benhida, K. Bougrin, Solvent-free regioselective synthesis of novel isoxazoline and pyrazoline N-substituted saccharin derivatives under microwave irradiation, Chem. Heterocycl. Compd. 52 (2016) 31–40.
[25] Z. Gordi, M. Vazan, Natural kaolin as an efficient recyclable catalyst for the synthesis of new 2,4-disubstituted quinolones, Iran. J. Catal. 6 (2016) 75–80.
[26] S. Perrone, A. Salomone, A. Caroli, A. Falcicchio, C. Citti, G. Cannazza, L. Troisi, Stereoselective synthesis of α-alkylidene β-oxo amides by palladium-catalyzed Carbonylation, European J. Org. Chem. 2014 (2014) 5932–5938.
[27] R. He, X. Jin, H. Chen, Z.-.T. Huang, Q.-.Y. Zheng, C. Wang, Mn-Catalyzed Three--Component Reactions of Imines/Nitriles, Grignard Reagents, and Tetrahydrofuran: an Expedient Access to 1,5-Amino/Keto Alcohols, J. Am. Chem. Soc. 136 (2014) 6558–6561.
[28] S. Sithambaram, R. Kumar, Y. Son, S. Suib, Tandem catalysis: direct catalytic synthesis of imines from alcohols using manganese octahedral molecular sieves, J. Catal. 2 (2008) 269–277.
[29] Z. Jiao, X. Feng, B. Liu, G.Zhang F.Chen, Y. Jiang, Enantioselective Strecker reactions between aldimines and trimethylsilyl cyanide promoted by chiral N, N ′ -dioxides, Eur. J. Org. Chem. 19 (2003) 3818–3826.
[30] Y.Q. Cao, Z. Dai, B.H. Chen, R. Liu, Sodium borohydride reduction of ketones, aldehydes and imines using PEG400 as catalyst without solvent, J. Chem. Technol. Biotechnol. 7 (2005) 834–836.
[31] M.M.A.R. Moustafa, B.L. Pagenkopf, Ytterbium triflate catalyzed synthesis of alkoxy-substituted donor–acceptor cyclobutanes and their formal [4 + 2] cycloaddition with imines: stereoselective synthesis of piperidines, Org. Lett. 12 (2010) 4732–4735.
[32] M. Kammoun, H.B. Salah, M. Damak, Synthesis and Reactivity Study of two New Dihydroisoquinoline-Derived Oxaziridines, Synth.Commun 41 (2011) 1520–1528.
[33] R. Aydi, M. Kammoun, Synthesis and Reactivity of Two New Trichloromethyl Substituted Dihydroisoquinoline-Derived Oxaziridines, Synth. Commun. 46 (2016) 134–144.
[34] R. Aydi, A.B. Gara, R. Chaaben, H.B. Saad, L. Fki, A. ElFeki, H. Belghith, K. Belghith, Kammoun M, Inhibition of key digestive enzymes related to hyperlipidemia and protection of liver-kidney functions by Cystoseira crinita sulphated polysaccharide in high-fat diet-fed rats, Biomed. Pharmacother. 82 (2016) 660–668.
[35] A. Selmi, R. Aydi, P. Mosset, R. Grée, M. Kammoun, Synthesis and reactivity of new dihydroisqunoline-derived oxaziridines, ARKIVOC v (2019) 108–120.
[36] S. Falah, R.Aydi F.Abdmouleh, B. Hamdi, M.El Arbi, M. Kammoun, Synthesis, crystal structure study, and antimicrobial evaluation activity of aryl-substituted dihydroisoquinoline oxaziridine, J. Mol. Struct. 1205 (2020) 127592.
[37] V.S. Shklyaev, B.B. Aleksandrov, G.I. Legotkina, M.I. Vakhrin, M.S. Gravrilov, A.A.G. Mikhailovskii, Synthesis and acylation of tertiary enamines: 1,2,3,4-tetrahydroisoquinoline derivatives, Chem. Heterocyclic.Comp. 24 (1983) 772–775.
[38] A.Mc Coubey, D.W. Mathieson, Iso-quinolines, part III: the nitration of 3,4-dihydroand 1,2,3,4-tetrahydro-isoquinolines, J. Chem. Soc. 51 (1951) 2851–2853.
[39] L. Bohé, M. Kammoun, Design of a highly efficient catalyst for the oxaziridinium mediated epoxidation of olefins by oxone, Tetrahedron Lett. 45 (2004) 747–751.
[40] S. Bhagani, V. Kapil, M.D. Lobo, hypertens. Med. 46 (2018) 509–515.
[41] C.-.L. Jao, S.-.L. Huang, K.-.C. Hsu, Angiotensin I-converting enzyme inhibitory peptides: inhibition mode, bioavailability, and antihypertensive effects, Bio Medicine 2 (2012) 130–136.
[42] L. Paiva, E. Lima, A.I. Neto, J. Baptista, Angiotensin I-converting enzyme (ACE) inhibitory activity of Fucus spiralis macroalgae and influence of the extracts storage temperature—a short report, J. Pharm. Biomed. Anal. 131 (2016) 503–507.
[43] D.J. Kuster, G.R. Marshall, Validated ligand mapping of ACE active site, J. Comput. Aided Mol. Des. 19 (2005) 609–615.
[44] A. Altomare, M.C. Burla, M. Camalli, G. Cascarano, C. Giacovazzo, A. Guagliardi, A.G.G. Moliterni, G. Polidori, R. Spagna, A new tool for crystal structure determination and refinement, J. Appl. Cryst. 32 (1999) 115–119.
[45] G.M. Sheldrick, A short history of SHELX, Acta Cryst A64 (2008) 112–122.
[46] F.L. Hirshfeld, Theor. Chim. Acta. 44 (1977) 129–138.
[47] M.A. Spackman, D. Jayatilaka, CrystEngComm. 11 (2009) 19–32.
[48] S.K. Wolff, D.J. Grimwood, J.J. McKinnon, M.J. Turner, D. Jayatilaka, M.A. Spackman, CrystalExplorer (Version 3.1), University of Western Australia, 2012.
[49] Y. Nakamura, N. Yamamoto, K. Sakai, A. Okubo, S. Yamazaki, T. Takano, Purification and characterization of angiotensin I-converting enzyme inhibitors from sour milk, JDS 78 (1995) 777–783.
[50] G.M. Morris, R. Huey, W. Lindstrom, M.F. Sanner, R.K. Belew, D.S. Goodsell, A.J. Olson, AutoDock4 and AutoDockTools4: automated docking with selective receptor flexibility, J. Comput. Chem. 30 (2009) 2785–2791.
[51] O. Trott, A.J. Olson, AutoDock Vina: improving the speed and accuracy of docking with a new scoring function, efficient optimization and multithreading, J. Comput. Chem. 31 (2010) 455–461.
[52] T. Gaillard, Evaluation of AutoDock and AutoDock Vina on the CASF-2013 benchmark, J. Chem. Inf. Model. 58 (2018) 1697–1706.
[53] R. Wang, L. Lai, S. Wang, Further development and validation of empirical scoring functions for structure-based binding affinity prediction, J. Comput. Aided Mol. Des. 16 (2002) 11–26.
[54] J.L. Velázquez-Libera, F. Durán-Verdugo, A. Valdés-Jiménez, G. Núñez-Vivanco, J. Caballero, LigRMSD: a web server for automatic structure matching and RMSD calculations among identical and similar compounds in protein-ligand docking, Bioinformatics 36 (2020) 2912–2914.